# Lectures in Paleomagnetism - DRAFT

Lisa Tauxe
Suggested Citation:
Lisa Tauxe, "Lectures in Paleomagnetism", 2005, Essayo Press,
http://repositories.cdlib.org/sio/library/8

April 3, 2005

# Chapter 8

# Applied Rock (Environmental) Magnetism

**Suggested Reading**

For background:
Chapter 1: Maher, B and Thompson, R., 1999.
Chapter 4: Evans and Heller 2003

## 8.1 Introduction

There is a lively field within paleomagnetism that attempts to exploit the dependence of rock magnetic parameters on concentration, grain size and mineralogy for the purpose of gleaning information about past (and present) environments. Applications in applied rock magnetism *(environmental magnetism)* run from detection of industrial pollution to characterizing climatic change across major climatic events to constraining rainfall variations across Asia during the Quaternary. In this lecture we will review the basic tool-kit used by environmental magnetists and illustrate various applications with examples.

## 8.2 Applied rock magnetism toolkit

There are four basic methodologies involved in most applied rock magnetism studies: imaging of magnetic separates, hysteresis parameter estimation, thermomagnetic measurements (including Curie Temperature determination and low temperature measurements) and anhysteretic remanence (ARM) measurements. Imaging is done using optical, scanning electron and transmission electron microscopes (see e.g., Figure 8.1a) on magnetic separates, or thin sections. Hysteresis measurements (including magnetic susceptibility) are made on vibrating sample magnetometers (VSMs), alternating gradient force magnetometers (AGFMs: see Lecture 7), and susceptibility meters (Figure 8.1b) of various sorts. These measurements can be done as a function of frequency or temperature. Thermomagnetic measurements are made on a "Curie Balance" (Figure 8.1c) which measures saturation magnetization as a function of temperature. ARMs are measured using an instrument that applies a large, alternating field (an AF demagntetizer) in the presence of a small DC bias field (see Lecture 5).

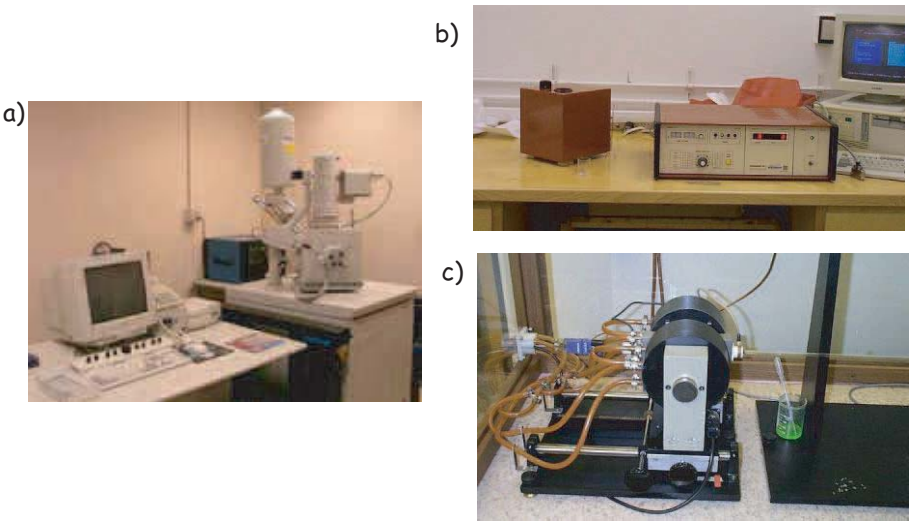


Figure 8.1: Some of the workhorse instruments of the practicing environmental magnetist. a) A scanning electron microscope. b) A susceptibility meter. c) A curie balance.

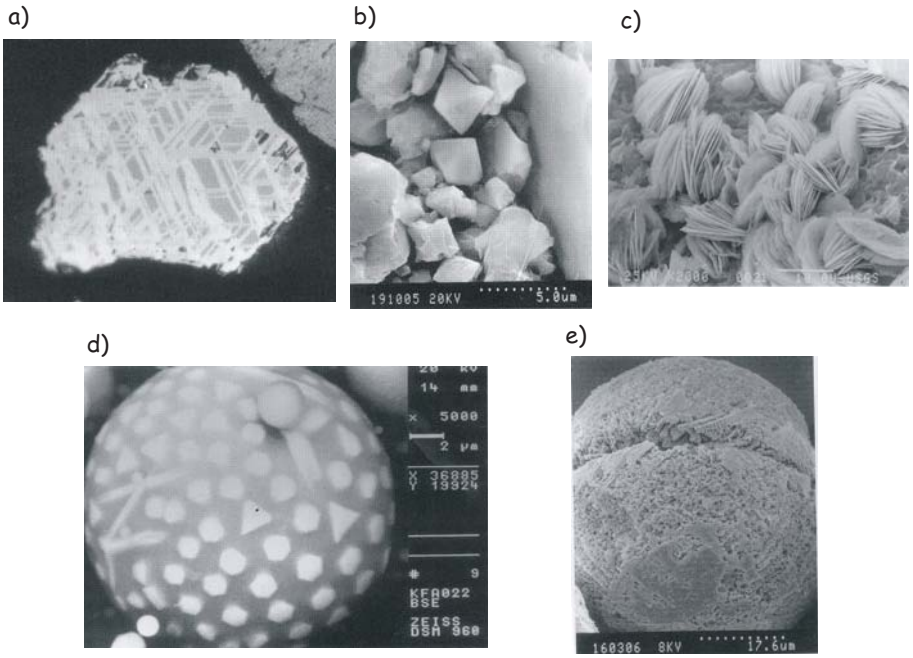


Figure 8.2: Images of magnetic phases from Maher and Thompson (1999) . a) 300 $\mu$m titanomagnetite grain of igneous origen showing high temperature exsolution lamellae b) Detrital and aeolian (titano)magnetites from Chinese Loess. (from Maher and Thompson, 1999). c) Hematite rosettes on a smectite surface. d) Backscatter SEM image of fly-ash spherule. The bright grains are iron rich particles embedded in a silicate matrix. e) Silicate spherule with dendrites of Fe-rich material of cosmic origin, showing characteristic pitting of the surface.

### 8.2.1 Images

Images of magnetic phases are used to constrain the origin of the magnetic phases. Igneous (Figure 8.2a), detrital or aeolian (Figure 8.2b), authigenic (Figure 8.2c), biogenic (Lecture 6), anthropogenic (Figure 8.2d) and cosmic (Figure 8.2e) sources all have distinctive ear-marks, so actually looking at the particles in question can provide invaluable information.

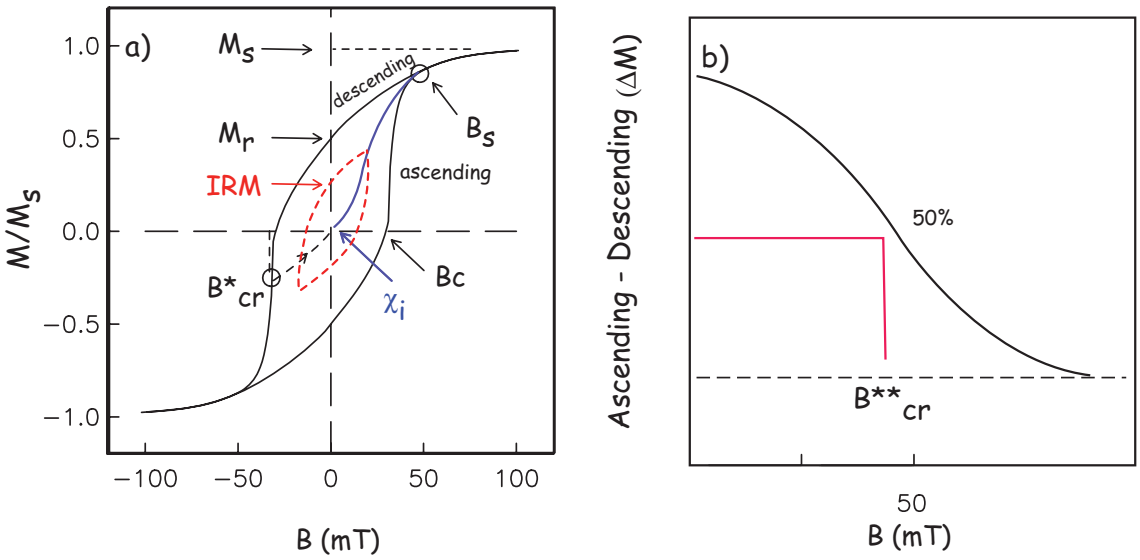


Figure 8.3: Definition of various hysteresis parameters.

### 8.2.2 Hysteresis parameter estimation

Hysteresis behavior is strongly controlled by mineralogy and grain size, hence hysteresis loops have the potential to help constrain the makeup of a given rock specimen. The hysteresis loop of a given sample will be the sum of all the curves generated by the individual grains. Each population of grains with a consistent coercivity spectrum will leave its imprint on the resulting loop.

We have already encountered hysteresis loops in Lecture 7 and many of the associated parameters that characterize them. There are a few more, however, that are useful in environmental magnetism (see Figure 8.3).

The slope relating magnetization and applied (low) fields is called the initial magnetic susceptibility ($\chi_i$) (see Lectures 1 and 3). This is a reversible measurement and if the field is low enough, the magnetization will return to its initial state when the field is turned off.

Because the response to an external field is greatly enhance if a particle is superparamagnetic, SP grains are hugely more susceptible than an equivalently sized SD grain. The definition of whether a given grain is SP or not depends on the time scale of observation, so a grain can be SP over a long period (and come into equilibrium with the applied field) but be SD over a shorter time scale (and have only a sluggish response to a small applied field). Therefore $\chi_i$ is strongly frequency dependent (as well as being strongly temperature dependent). Some instruments allow the measurement of $\chi_i$ at various frequencies allowing the definition of the so-called frequency

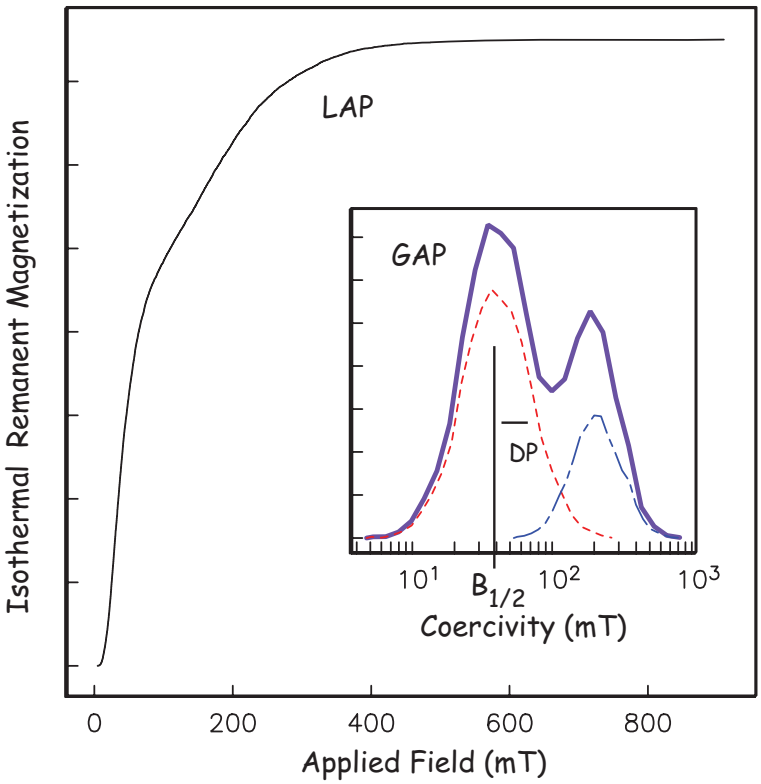


Figure 8.4: Theoretical curve for the acquisition of IRM with two magnetic components with different coercivfity spectra (see insert). The acquisition curve can be differentiated to get the heavy solid line in the insert and then decomposed into the different components assuming some distribution of coercivity (in this case log-normal). The main plot is a "linear acquisition plot" (LAP) and the heavy solid line in the inset is a "gradient of acquisition plot" (GAP) in the terminology of Kruiver et al. (2001). $B_{1/2}$ and $DP$ are the fields required to magnetize half the population and the "dispersion parameter" of Robertson and France (1994). Note that $B_{1/2}$ is the same as $B'_{cr}$ if there is only one population of coercivities.

dependent susceptibility or $\chi_{fd}$. This is often used to estimate the contribution of SP particles to the total susceptibility.

As the applied magnetic field increases, individual particles will reach their flipping fields, or undergo some other irreversible reorganization of spin states (rearranging domain walls, etc.). Saturation magnetization ($M_s$) is the magnetization measured in the presence of a saturating field ($B_s$). This measurement must often be "corrected" for the contribution of paramagnetic minerals whose *high field susceptibility* $\chi_{hf}$ must be subtracted. Fortunately, paramagnetic behavior is linear up to several tesla so can usually be estimated and removed. If we subtract the high field susceptibility (which is only the paramagnetic contribution) from the initial susceptibility, we can estimate the contribution of the ferrimagnetic (*sensu lato*) particles or $\chi_{ferri}$.

Susceptibility can also be measured as a function of the orientation of the specimen with respect to the applied magnetic field. If the susceptibility is independent of orientation, it is said to be isotropic. Anisotropic orientations of magnetic minerals can lead to an anisotropic magnetic susceptibility response which in turn can be interpreted in terms of preferred orientation of magnetic

phases. This topic will be addressed in later lectures.

The portion of the hysteresis loop that is recorded while the field is ramping up is called the *ascending* loop and the return portion recorded as the field is ramping down is the *descending* loop. Once the field is high enough, irreversible changes in the magnetization of the sample take place and the magnetization will no longer return to its initial state after the field is switched off; it displays hysteresis (see Lecture 7). The magnetization thus acquired is an IRM (see Lecture 5). The remanence remaining after application of a saturating field was termed saturation remanence $M_r$ in Lecture 7 (also known as $M_{rs}$ or $M_{sr}$ in the literature). It is also synonymous with the saturation IRM (sIRM).

As mentioned in Lecture 5, the coercive field ($B_c$) is that field required to reduce the net magnetization to zero and the bulk coercivity of remanence ($B_{cr}$) is the field necessary to flip half the magnetic moments (so when the field is turned off, the remanence is reduced to zero). Two ways of estimating $B_{cr}$ were described in Lecture 5 ($B_{cr}$ and $B'_{cr}$. A third way is the intersection method described in Lecture 7 ($B*_{cr}$). A fourth way is the $\Delta M$ method illustrated in Figure 8.3b whereby the difference between the ascending and descending loops ($\Delta M$) from Figure 8.3a is plotted versus applied field. The field at which the value of $\Delta M$ is 50% of the maximum is here called $B**_{cr}$.

Robertson and France (1994) suggested that if populations of magnetic materials have generally log-normally distributed coercivity spectra and if the IRM is the linear sum of all the contributing grains, then an IRM acquisition curve could be "unmixed" into the contributing components. The basic idea is illustrated in Figure 8.4 whereby two components each with log normally distributed coercivity spectra (see dashed and dashed-dotted lines in the inset) create the IRM acquisition curve shown. Thus by obtaining a very well determined IRM acquisition plot (the "linear acquisition plot" or LAP in Figure 8.4 using the terminology of Kruiver et al., 2001), one could first differentiate it to get the "gradient acquisition plot" or GAP using the terminology of Kruiver et al., 2001 (heavy solid line in the inset to Figure 8.4 ). This then can be "unmixed" to get the parameters of the contributing components such as the mean and standard deviation of the log-normal distribution (called $B_{1/2}$ and $DP$ respectively by Robertson and France, 1999). Note that $B_{1/2}$ is synonymous with $B_{cr}$ if there is only one population of coercivities. Also, other forms of magnetic remanence (e.g., ARM), demagnetization as well as acquisition, and other distributions are also possible as are fancier methods of inversion (see e.g., Egli 2003).

### 8.2.3 Combining thermal and isothermal information for rock magnetic characterization

Another very useful technique for characterizing the magnetic mineralogy in a sample is the Lowrie 3D IRM technique (Lowrie, 1990). Some important magnetic phases in geological materials (Table 1; Lecture6) are magnetite (maximum blocking temperature of ~580°C, maximum coercivity of about 0.3 T), hematite (maximum blocking temperature of ~ 675°C and maximum coercivity much larger than 5 T), goethite (maximum blocking temperature of ~ 125°C and maximum coercivity of much larger than 5 T), and various sulfides. The relative importance of these minerals in bulk samples can be constrained by a simple trick that exploits both differences in coercivity and unblocking temperature (Lowrie, 1990).

The Lowrie "3D IRM test" proceeds as follows:

- Apply an IRM along three orthogonal directions in three different fields. The first field, applied along $\mathbf{X}_1$, should be sufficient to saturate all the minerals within the sample

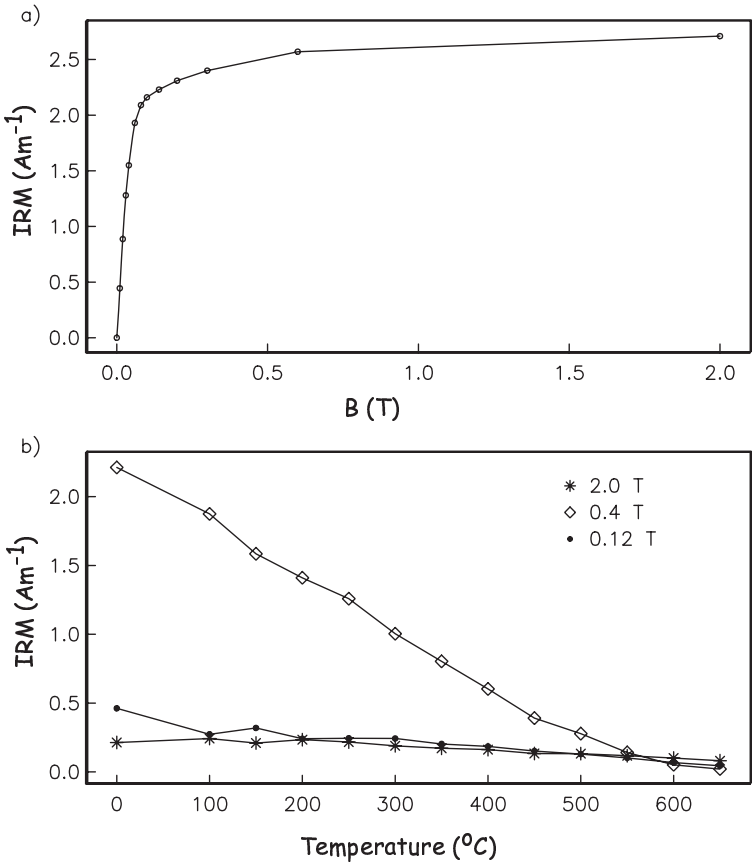


Figure 8.5: a) Acquisition of IRM ($M_r$). After applying a field of 2 T, the sample was subjected to two additional IRMs: 0.4 T and 0.12 T along orthogonal axes. b) Thermal demagnetization of a 3-axis IRM. Each component is plotted separately.

and is usually the largest field achievable in the laboratory (say 2 T). The second field, applied along $\mathbf{X}_2$, should be sufficient to saturate magnetite, but not to realign high coercivity phases, such as goethite or fine-grained hematite (say 0.4 T). The third IRM, applied along $\mathbf{X}_3$, should target low coercivity minerals and the field chosen is typically something like 0.12 T.

• The composite magnetization can be characterized by determining the blocking temperature spectra for each component. This is done by thermally demagnetizing the sample and plotting the magnitude of the three cartesian components $(x_1, x_2, x_3)$ versus demagnetizing temperature.

An example of 3D IRM data are shown in Figure 8.5. The curve is dominated by a mineral with a maximum blocking temperature of between 550° and 600°C and has a coercivity less than 0.4 T, but greater than 0.12 T. These properties are typical of magnetite (Table 1; Lecture 6). There is a small fraction of a high coercivity (>0.4 T) mineral with a maximum unblocking temperature > 650°C, which is consistent with the presence of hematite (Table 1; Lecture 6).

IRM and ARM acquisition and demagnetization curves could be a rich source of information about the magnetic phases in rocks. However, these are extremely time consuming to measure

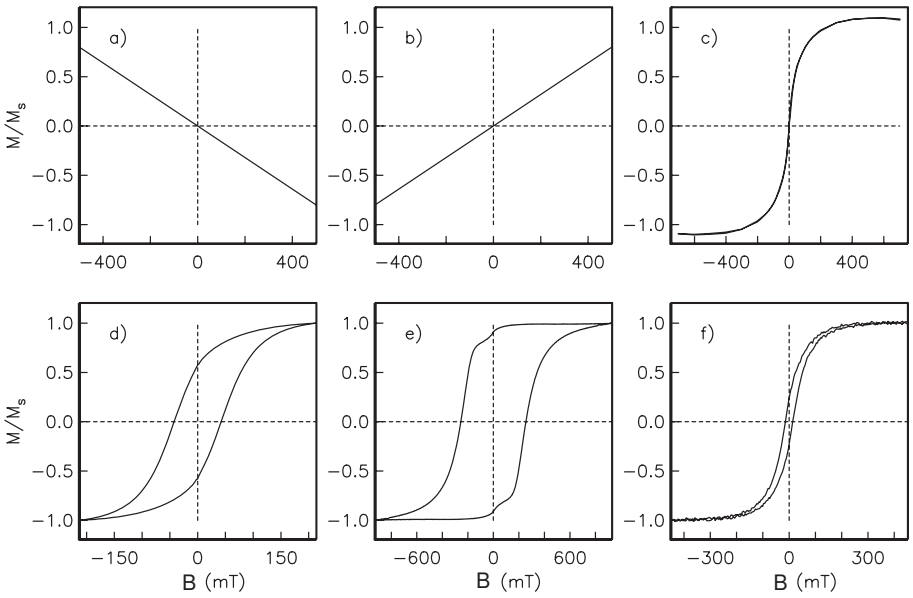


Figure 8.6: Hysteresis loops of end-member behaviors: a) diamagnetic, b) paramagnetic, c) superparamagnetic (data for submarine basaltic glass), d) uniaxial, single domain, e) magnetocrystalline, single domain, f) "pseudo-single domain".

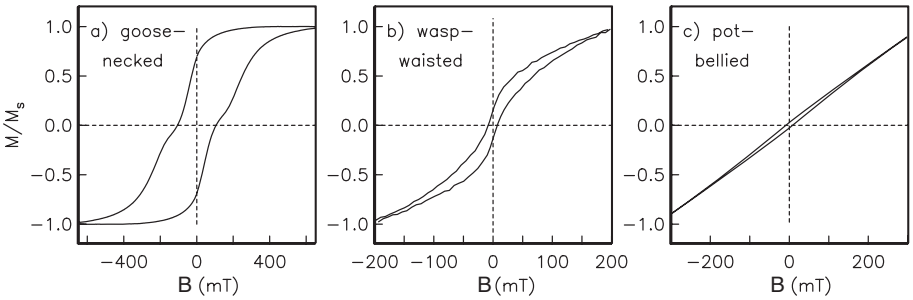


Figure 8.7: Hysteresis behavior of various mixtures: a) magnetite, and hematite, b) SD/SP magnetite (data from Tauxe et al. 1996), c) another example of SD/SP magnetite.

taking hours for each one. Hysteresis loops on the other hand are quick, taking about 10 minutes to measure the outer loop. In principle, the same information could be had from hysteresis loops as in the IRM acquisition curves.

Hysteresis loops, like IRM acquisition curves are the sum of all the contributing particles in the sample. There are several basic types of loops which are recognized the "building blocks" of the hysteresis loops we measure on geological materials. We illustrate some of the building blocks of possible hysteresis loops in Figure 8.6. Figure 8.6a shows the negative slope typical of diamagnetic material such as carbonate or quartz, while Figure 8.6b shows a paramagnetic slope. Such slopes are common when the sample has little ferromagnetic material and is rich in iron-bearing phases such as biotite or clay minerals.

When grain sizes are very small, a sample can display superparamagnetic "hysteresis" behavior (Figure 8.6c). The SP curve follows a Langevin function $L(a)$ (see Lecture 7) where $a$ is $M_s vB/kT$,

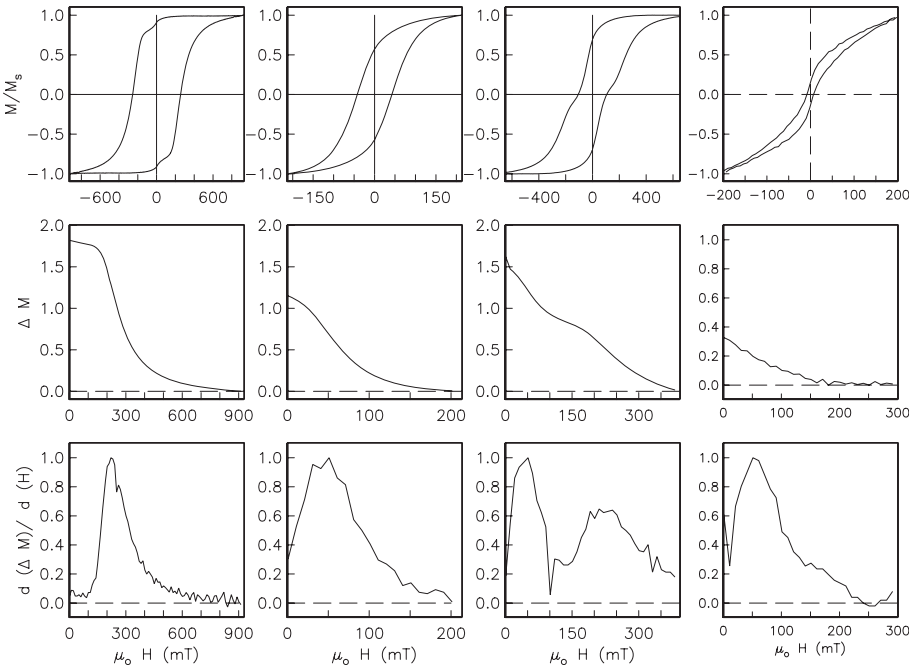


Figure 8.8: Top panels: hysteresis curves, middle panels: $\Delta M$ curves and bottom panels: $d\Delta M/dH$ curves. From the left to right: hematite, SD magnetite, hematite plus magnetite, and SD plus SP magnetite.

but integrates over the distribution of $v$ in the sample.

Above some critical volume, grains will have relaxation times that are sufficient to retain a stable remanence (Lecture 5). As discussed in Lecture 7, populations of randomly oriented stable grains can produce hysteresis loops with a variety of shapes, depending on the origin of magnetic anisotropy and domain state. We show loops from samples that illustrate representative styles of hysteresis behavior in Figure 8.6d-f. Figure 8.6d shows a loop characteristic of samples whose remanence stems from SD magnetite with uniaxial anisotropy. In Figure 8.6e, we show data from specular hematite whose anisotropy is magnetocrystalline in origin (hexagonal within the basal plane). Note the very high $M_r/M_s$ ratio of nearly one. Finally, we show a loop that has lower $M_r/M_s$ ratios than single domain, yet some stability. Loops of this type have been characterized as *pseudo-single domain* PSD (Figure 8.6f). We now know that PSD behavior is typical of vortex remanence state particles.

In the messy reality of geological materials, we often encounter mixtures of several magnetic phases and/or domain states. Such mixtures can lead to distorted loops, such as those shown in Figure 8.7. In Figure 8.7a, we show a mixture of hematite plus SD-magnetite. The loop is distorted in a manner that we refer to as *goose-necked*. Another commonly observed mixture is SD plus SP magnetite which can result in loops that are either *wasp-waisted* (see Figure 8.7b) or *pot-bellied* (see Figure 8.7c).

Considering the loops shown in Figure 8.7, we immediately notice that there are two distinct causes of loop distortion: mixing two phases with different coercivities and mixing SD and SP domain states. We differentiate the two types of distortion as "goose-necked" and "wasp-waisted" (see Figure 8.7) because they look different and they mean different things.

Jackson et al. (1990) suggested that the $\Delta M$ curve (see Figure 8.3) could be differentiated to reveal different coercivity spectra contained in the hysteresis loop. The $\Delta M$ curve and its derivitive ($d\Delta M/dH$) are sensitive only to the remanence carrying phases, and not, for example, to the SP fraction, we can use these curves to distinguish the two sources of distortion. In Figure 8.8, we show several representative loops, along with the $\Delta M$ and $d\Delta M/dH$ curves. Distortion resulting from two phases with different coercivities (e.g., hematite plus magnetite or two distinct grain sizes of the same mineral) results in a "two humped" $d\Delta M/dH$ curve, whereas wasp-waisting which results from mixtures of SD + SP populations have only one "hump".

Jackson et al. (1990) also suggested a way to deal with noisy data using Fourier smoothing. This treatment is described in the appendix.

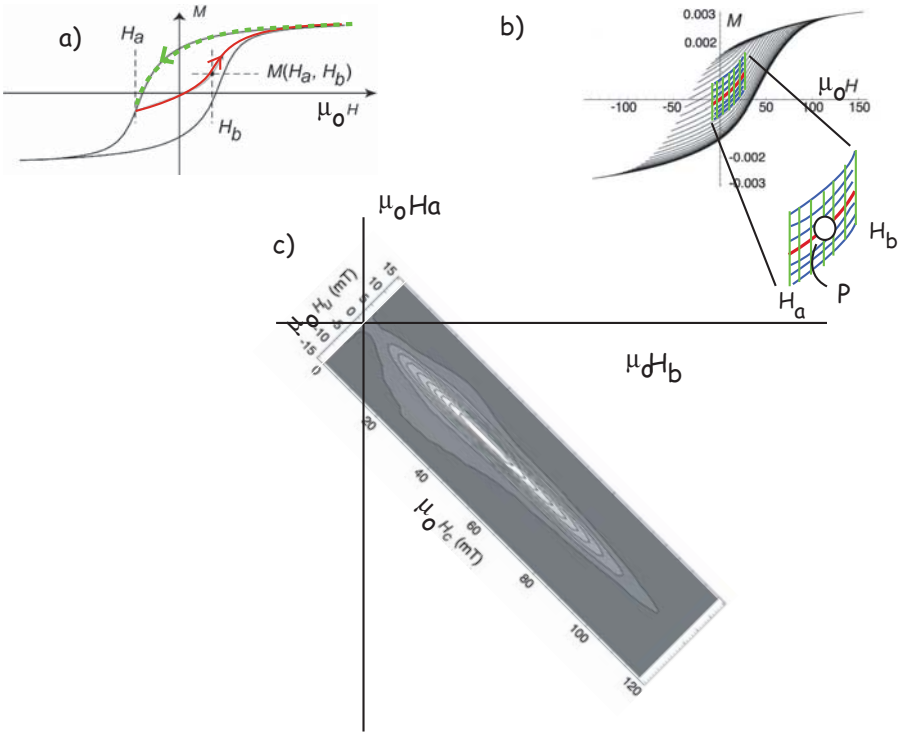


Figure 8.9: a) Dashed line is the descending magnetization curve taken from a saturating field to some field $H_a$. Red line is the first order reversal curve (FORC) from $H_a$ returning to saturation. At any field $H_b > H_a$ there is a value for the magnetization $M(H_a, H_b)$. b) A series of FORCs for a single domain assemblage of particles. At any point "P" there are a set of related curves making a 7x7 grid. A polynomial surface is fit to these data is estimated. c) A contour plot of the mixed second derivative of the polynomial surface evaluated for points $H_a, H_b$. (Redrawn from Pike et al., Phys. Earth Planet. Int., 126, 11-25. 2001). Note: all $H$s are actually $\mu_o H$.

Hysteresis loops can yield a tremendous amount of information yet much of this is lost by simply estimating the set of parameters $M_r, M_s, B_{cr}, B_c, \chi_i, \chi_{hf}$, etc.. Pike et al. (e.g., 1999) popularized the method of Mayergoyz (1986) or using so-called *First Order Reversal Curves* or FORCs to represent hysteresis data. In the FORC experiment, a sample is subjected to a saturating field, as in most hysteresis experiments. The field is lowered to some field $H_a$, then increased again through some value $H_b$ to saturation (see Figure 8.9a). [It is unfortunate that the FORC terminology has

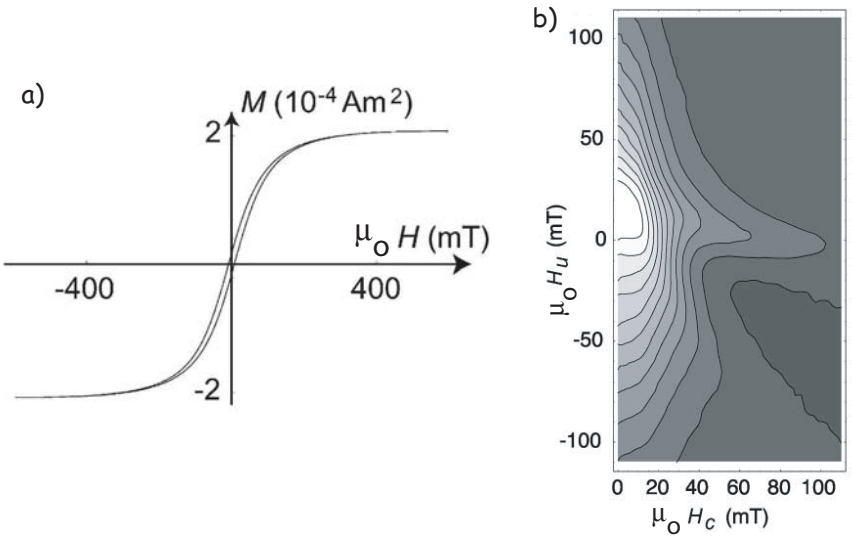


Figure 8.10: a) Hysteresis loop for a large, stressed gain of magnetite prior to annealing. b) FORC diagram from same. (Redrawn from Pike et al., 2001).

chosen to use $H_a$, yet routinely neglects the necessary $\mu_o$ to render these field values in tesla...] The magnetization curve between $H_a$ and $H_b$ is a "FORC". A series of FORCs (see Figure 8.9b) are generated to the desired resolution.

To transform FORC data into some useful form, they are gridded as in the inset in Figure 8.9c. In this example, we take a curve (in red) with its three neighbors on either side (in green), for a smoothing factor of $SF = 3$. The data in the box are fit with a polynomial surface of the form:

$$a_1 + a_2 H_a + a_3 H_a^2 + a_4 H_b + a_5 H_b^2 + a_6 H_a H_b$$

where the $a_i$ are fitted coefficients. The coefficient $-a_6(H_a, H_b)$ is contoured as in the Figure 8.9b and is a good approximation for the second derivative of the polynomial surface at P (Figure 8.9b). A FORC diagram is the contour plot rotated such that $H_c = (H_b - H_a)/2$ and $H_u = (H_a + H_b)/2$. Please note that because $H_a < H_b$, data are only possible for positive $H_c$.

To interpret these diagrams in a meaningful way, let us return to Lecture 7. Imagine we travel down the descending magnetization curve (dashed line in Figure 8.9a) to a particular field $\mu_o H_a$ less than the smallest flipping field in the assemblage. If the particles are single domain, the behavior is reversible and the first FORC will travel back up the descending curve. It is only when $|\mu_o H_a|$ exceeds the flipping field of some of the particles that the FORC will trace a new curve on the inside of the hysteresis loop. In the simple single domain, non-interacting, uniaxial magnetite case, the FORC density in the quadrants where $H_a$ and $H_b$ are of the same sign must be zero. Indeed, FORC densities will only be non-zero for the range of flipping fields because these are the bounds of the flipping field distribution. So the diagram in Figure 8.9c is nearly that of an ideal uniaxial SD distribution.

Consider now the case in which a particle has domain walls. Walls can move much more easily than flipping the moment of an entire grain coherently. In fact, as we discussed in Lecture 7, they begin to move in small jumps (from LEM to LEM) as soon as the applied field changes. If a wall

nucleates while the field is decreasing and the field is then ramped back up, the magnetization curve will not be reversible, even though the field never changed sign or approached the flipping field for coherent rotation. The resulting FORC for such behavior would have much of the action in the region where $H_a$ is positive. When transformed to $H_u$ and $H_c$, the diagram will have the highest densities for small $H_c$ but over a range of $\pm H_u$ as shown in Figure 8.10.

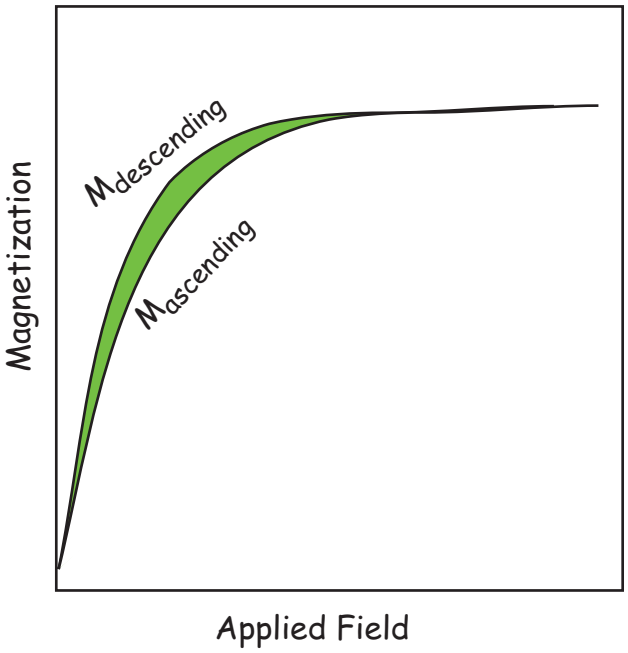


Figure 8.11: Illustration of a Zero FORC (ZFORC) whereby the descending loop from satruation is terminated at zero field and the field is then ramped back up to saturation. The transient hysteresis (TH) of Fabian (2003) is the shaded area between the two curves.

### 8.2.4 Which FORC should you use?

FORC diagrams take hours to create while a single hysteresis loop takes minutes. In many cases the the most interesting thing one learns from FORC diagrams is the degree to which there is irreversible behavior when the field is reduced to zero then ramped back up to saturation (see Figure 8.11). Such irreversible behavior in what Yu and Tauxe (2004) call the "Zero FORC" or ZFORC can arise from particle interactions, domain wall jumps or from the formation and destruction of vortex structures in the magnetic grains.

Fabian (2003) defined a parameter called "transient hysteresis" which is the area between the ascending and descending loops of a ZFORC (shaded area in Figure 8.11). This is defined as:

$$TH = \sum_{0}^{B_s} [M_{descending} - M_{ascending}] \cdot \Delta B.$$

where $\Delta H$ is the field increment used in the hysteresis measurement. When normalized by $M_s$, TH has units of $B$ (tesla).

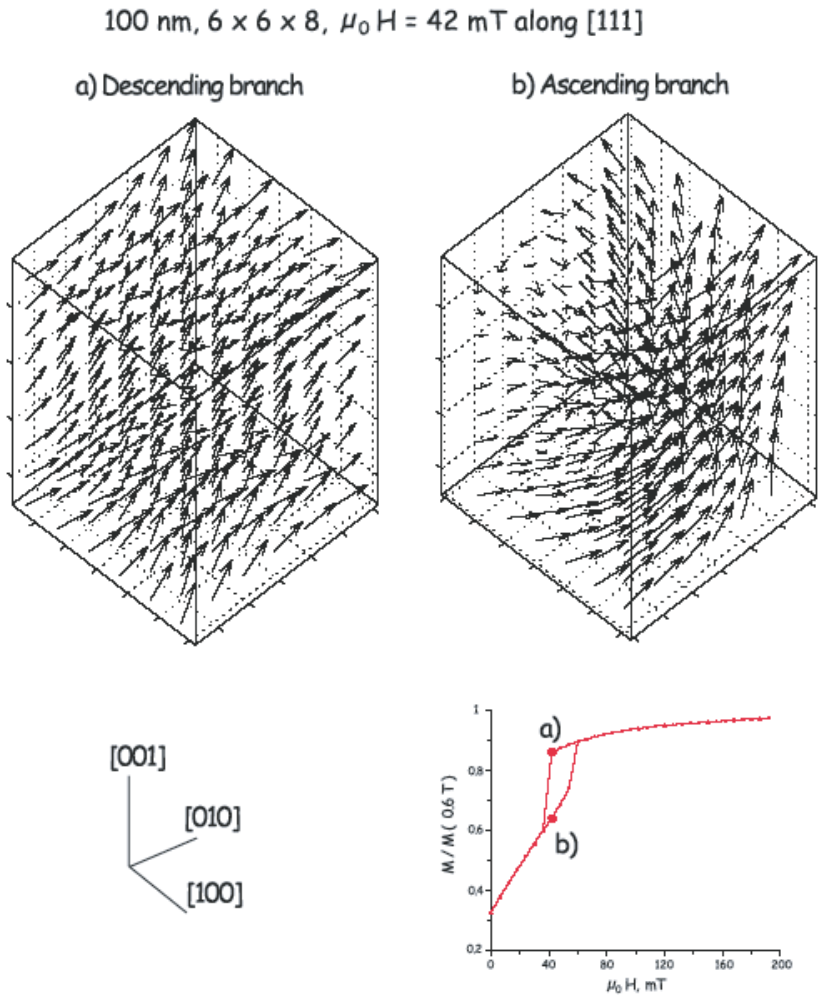


Figure 8.12: Example of source of transient hysteresis from micromagnetic modelling of a 100 nm particle undergoing a ZFORC experiment. (Figure from Yu and Tauxe, 2004.)

Transient hysteresis is thought to result from self demagnetization, for example shifting of domain walls or the formation and destruction of vortex structures. An example of what might be causing transient hysteresis at the macro scale is shown for micromagnetic modelling of a single particle in Figure 8.12 (Yu and Tauxe, 2004). The ZFORC starts and ends at saturation. On the descending loop, a vortex structure suddenly forms, at the point on the hysteresis loop labelled a), sharply reducing the magnetization. The magnetization state just before the jump is shown as snapshot labelled "descending branch". The vortex remains along the ascending branch until much higher fields (see snapshot labelled "ascending branch"). The irreversible behavior of millions of particles with different sizes and shapes leads to the total transient hysteresis of the macro specimen. In general, Tauxe and Yu (2004) showed that the larger the particle, the greater the transient hysteresis, until truly multi-domain behavior essentially closed the loop, precluding the observation of TH (or of a FORC diagram for that matter).

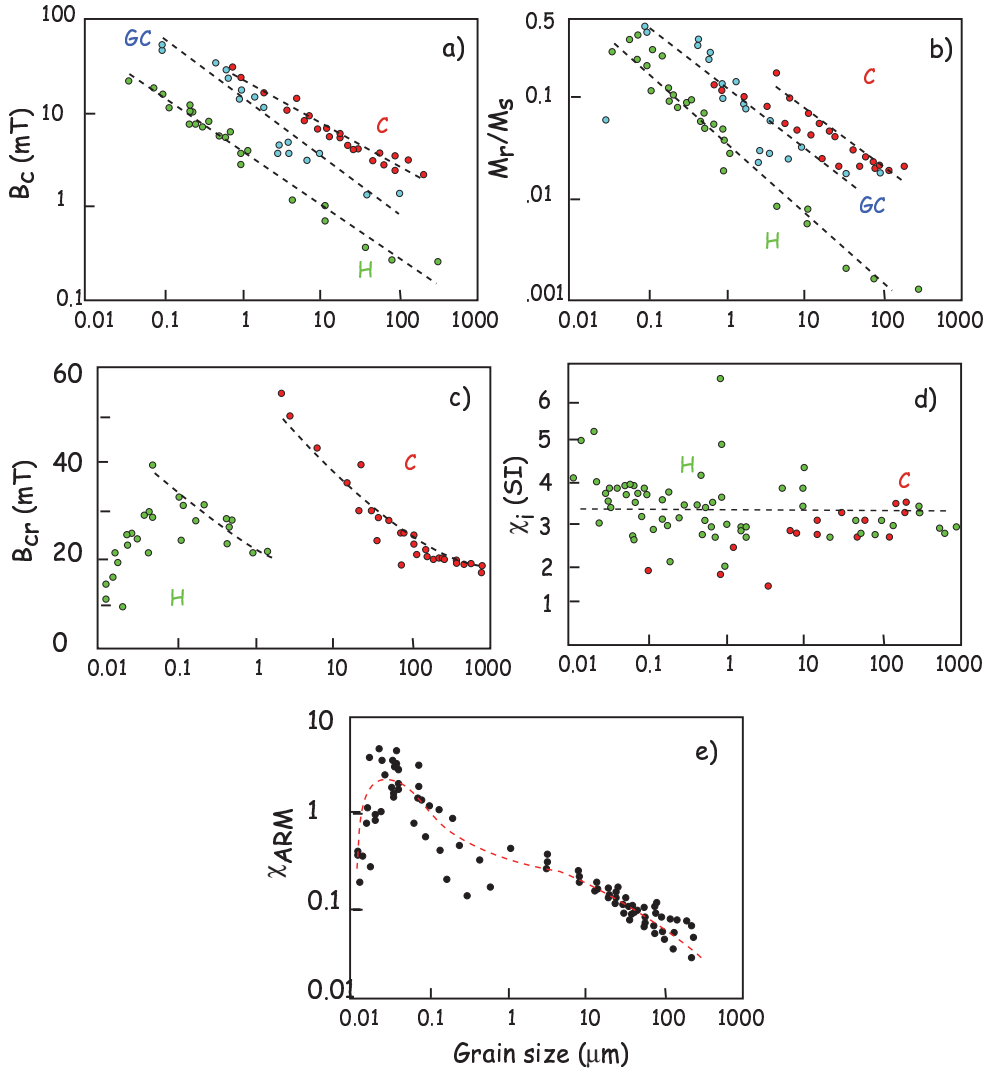


Figure 8.13: Grain size dependence in hysteresis parameters. Crushed grains (red) indicated by "C", glass ceramic grains (blue) indicated by CG; Hydrothermal grains (green) indicated by "H". a) Variation of coercive force ($B_c$). b) Variation of $M_r/M_s$. c) Variation of coercivity of remanence $B_{cr}$. (Data compiled by Hunt et al., 1995.) d) Variation of susceptibility with grain size. (Data compiled by Heider et al., 1996.) e) Variation in ARM with grain size. (Data of Dunlop and Argyle, 1997.)

## 8.3 Trends in hysteresis parameters with particle dimensions.

One holy grail of applied rock magnetism is a diagnostic set of measurements that will yield unambiguous grain size information. To this end, large amounts of hysteresis data have been collected on a variety of minerals that have been graded according to size and mode of formation. The most complete set of data are available for magnetite, as this is the most abundant magnetic phase in the world. There are three sources for magnetite typically used in these experiments: natural crystals that have been crushed and seived into grain size populatins, crystals that were grown by a glass ceramic technique and crystals grown from hydrothermal solution. In Figure 8.13a-c we show a compilation of grain size dependence of coercive force, remanence ratio, coercivity of remanence respectively. There is a profound dependence not only on grain size, but on mode of formation as well. Crushed particles tend to have much higher coercivities and remanence ratios than grown crystals, presumably because of the increased dislocation density which stabilizes domain walls in much the same manner as do voids. These abnormally high values disappear to a large extent when the particles are annealed at high temperature - a procedure which allows the dislocations to "relax" away.

The behavior of initial magnetic susceptibility is shown in Figure 8.13d. There is no strong trend with grain size over the entire range of grain sizes from single domain to multi-domain magnetite. Susceptibility is predicted to be sensitive to the SD/SP domain state transition, however, because in SP particles, the magnetization is unconstrained by magnetocrystalline or shape anisotropy energies, hence has a larger response to an applied field by a factor of $\ln(C\tau)$. Taking $C$ to be $10^{10}s^{-1}$ and $\tau$ to be order 100 s, we find a factor of $\sim 28$ enhancement of magnetic susceptibility for SP grains over an SD grain of the same volume. This is the basis for using frequency dependence to detect the contribution of SP grains to a population. Because SP behavior depends on the time scale of observation, particles may behave SP at lower frequencies and not at higher frequencies. Because $\tau$ is exponentially sensitive to temperature $\chi(T)$ often yields much more information than $\chi(f)$.

Grain size trends in ARM are shown in Figure 8.13e. This trend is very poorly constrained because ARM is also a strong function of concentration and the method by which the particles were prepared. Some (e.g. Banerjee et al., 1981) have suggested that the ratio of ARM (normalized by the DC field applied to get the so-called ARM susceptibility or $\chi_{ARM}$ to $\chi$ could be used to determine grain size in magnetite, but there are substantial practicle difficulties with this method, unless a great deal is known about concentration, origin of the minerals and magnetic mineralogy.

## 8.4 Parameter ratios

There is a bewildering array of parameter ratios that are in popular use in the applied rock and mineral magnetism literature: $M_r/M_s, B_{cr}/B_c, ARM/\chi, ARM/M_r, M_r/\chi, IRM(x)/M_r$. The ratios $M_r/M_s$ and $B_{cr}/B_c$ are sensitive to remanence state (SP, SD, flower, vortex, MD) and the source of magetic anisotropy (cubic, uniaxial, stress), hence reveal something about grain size and shape. For this reason Day et al., (1977) began plotting these ratios on a diagram that has since been called the "Day" plot (see e.g., Figure 8.14).

Day plots are divided into regions of supposedly SD, "PSD" and MD behavior using some theoretical bounds as guides (see Lecture 7). The designation PSD stands for *pseudo-single domain* and has $M_r/M_s$ ratios in between those characteristic of SD behavior (0.5 or higher) and MD (.05

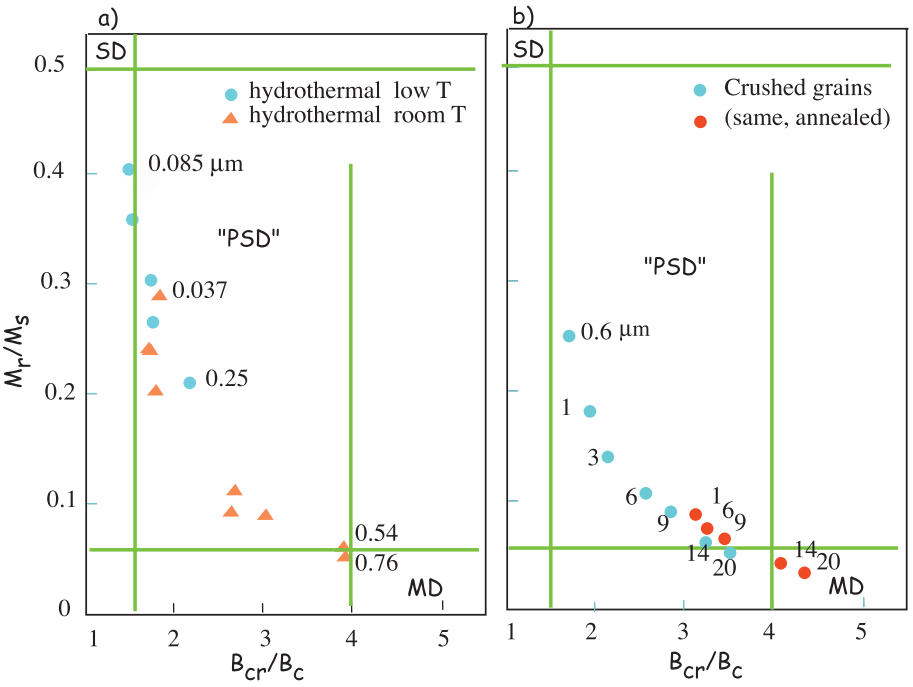


Figure 8.14: Day plot of hysteresis ratios versus grain size and mode of sample preparation. (Redrawn from Dunlop, 2002.)

or lower). In practice nearly all geological materials plot in the PSD box so the usefulness of the Day plot is limited.

Tauxe et al., (2002; see Figure 8.15) suggested that instead of the Day plot, $M_r/M_s$ could be plotted against $B_c$. This type of plot has been characterized to some extent using micromagnetic modeling techniques to aide in the interpretation of hysteresis data in terms of domain state and origin of magnetic anisotropy energy.

Ratios involving ARM and $\chi$ can be complicated because both of these parameters have ratio complicated behaviors themselves. ARM is a strong function of concentration and not monotonic with grain size. $\chi$ is a "garbage can" parameter that reflects everything in the sample to some extent. Under certain uncomplicated conditions, both of these parameters can be quite useful, but care should be exercised in their interpretation.

Ratios of a lower back-field IRM (IRM(-x)) to saturation IRM ($M_r$ or sIRM), the so-called *S-ratio*, can be used to quantify the ratio of hard (magnetized at saturation) to soft (remagnetized in the back field direction) minerals in a sample. IRM is less affected by particle interactions so behaves more linearly with concentration.

## 8.5 Applications

Rock magnetic parameters are relatively quick and easy to measure, compared to geochemical, sedimentological and paleontological data. When used judiciously, they can be enormously helpful in constraining a wide variety of climatic and environmental changes. There are two basic types of plots of the rock and mineral magnetic parameters discussed in this lecture: bi-plots and depth

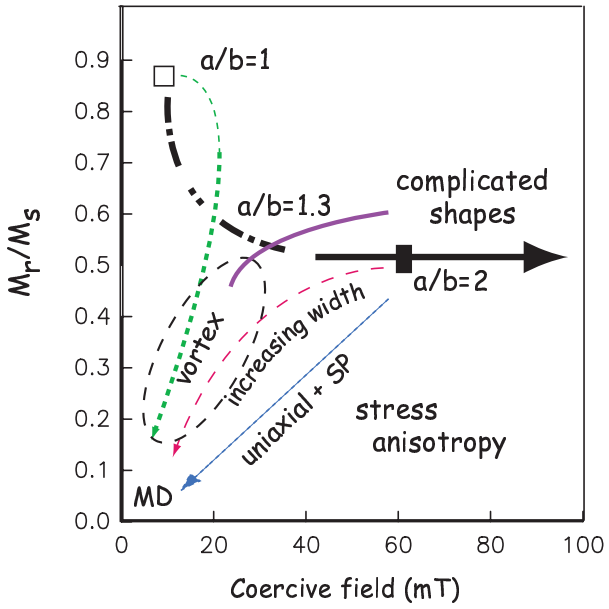


Figure 8.15: Interpretive diagram of $M_r/M_s$ versus coercive field. The open square is the theoretical location of an assemblage of magnetite particles with cubic anisotropy. As the particle grows in length (the length to width ratio $a/b$ approaches 1.5), the simulations plot follow the dash-dot trend. Assemblages with longer SD particles will follow the uniaxial trend indicated by the solid black arrow. SP-Uniaxial numerical simulations (SPUNS) predict the trend indicated by the blue dotted line (Tauxe et al., 1996). Assemblages with larger particle widths of equant grains follow the green dotted line; those of elongate particles follow the red dashed line. As particles become large enough for to be in the vortex remanent state, they plot in the region labelled "PSD". More complicated shapes, such as intersecting rods can give $M_r/M_s$ ratios above 0.5, yet have enormously high stability (region labelled complicated shapes. As these particles grow, their hysteresis data trend along the solid purple line. (From Tauxe et al., 2002.)

plots. Bi-plots, for example ARM versus $\chi$ have been in use since Banerjee et al. (1981) first proposed their use (see e.g., Figure 8.16). Biplots can be useful for detecting changes in grain size, concentration, mineralogy, etc. If for example, the data in a plot of $M_r$ verus $\chi$ plot on a line, it may be appropriate to interpret the dominant control on the rock magnetic parameters as changes in concentration alone.

Depth plots are useful for core correlation, variations in concentration, mineralogy and grain size as a function of depth. An example of a paleoceanographic application of rock magnetism from Hartl et al. (1995) is illustrated in Figures 8.17 and 8.18. Trends in isotopes and carbonate are shown in Figure 8.17. These indicate a major change in the environment at the end of the Eocene.

IRM and $\chi$ were measured as well. The pronounced changes in carbon isotopes appeared to be mirrored in the rock magnetic variations. It was tempting to attribute these variations to be simply related to the complimentary changes in % $CaCO_3$ because both IRM and $\chi$ are approximately linear functions of concentration. However, a look at the bi-plot of IRM versus $\chi$ (Figure 8.18) shows a more complicated and interesting picture. If the variations in these parameters were only caused by changes in concentration, the bi-plot would show a straight line. Instead, the data plot

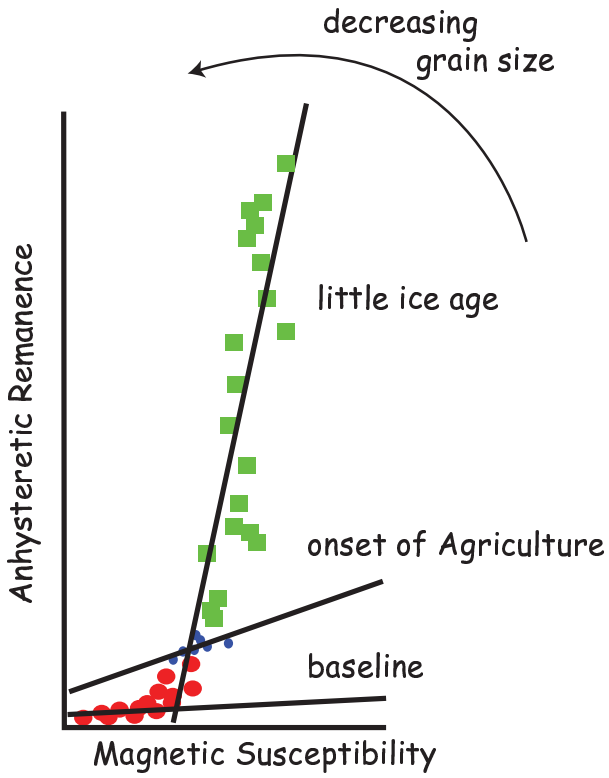


Figure 8.16: Plot of ARM versus magnetic susceptibility for a core from Minnesota. The different slopes are correlated with major climatic and anthropogenic events during the Holocene. (Redrawn from Banerjee et al., 1981).

along two lines with the Eocene data having a different slope and an overall larger constribution to $\chi$ than the Oligocene group. As mentioned earlier in the lecture, $\chi$ is a very strong function of the fraction of superparamagnetic grains to the population and Hartl et al. (1995) argue that there is a shift in grain size associated with the Eocene Oligocene boundary, with a greater fraction of SP grains in the Eocene than in the Oligocene. A change in magnetic grain size can be the result of changes in the pore water chemistry resulting from changes in organic carbon delivery. This mechanism is consistent with the carbon isotopic variations shown in Figure 8.17.

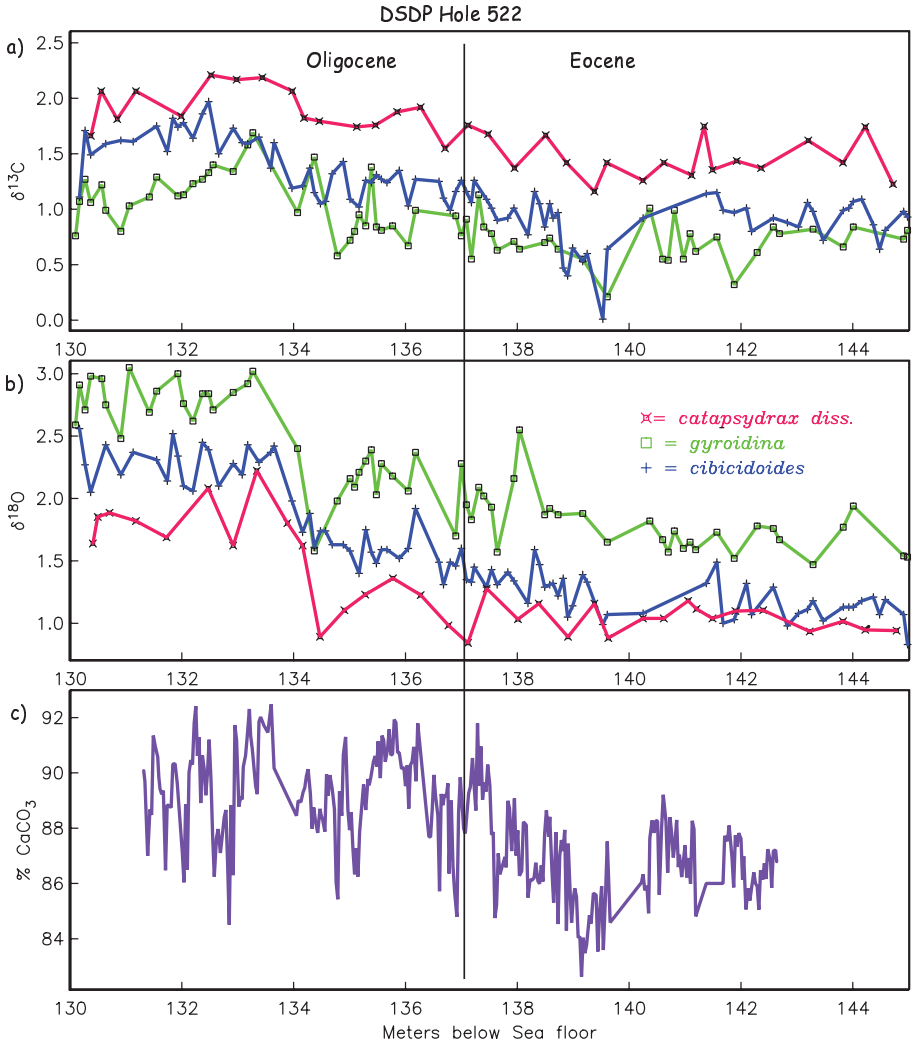


Figure 8.17: a) $\delta^{13}$C and b) $\delta^{18}$O isotopic variations of benthic and planktonic foraminifera from Site 522. c) Variations in percent calcium carbonate . The Eocene Oligocene boundary is defined as the last occurrence of *Hantkenina spp.* at 137 meters below sea floor. Figure redrawn from Hartl et al. (1995).

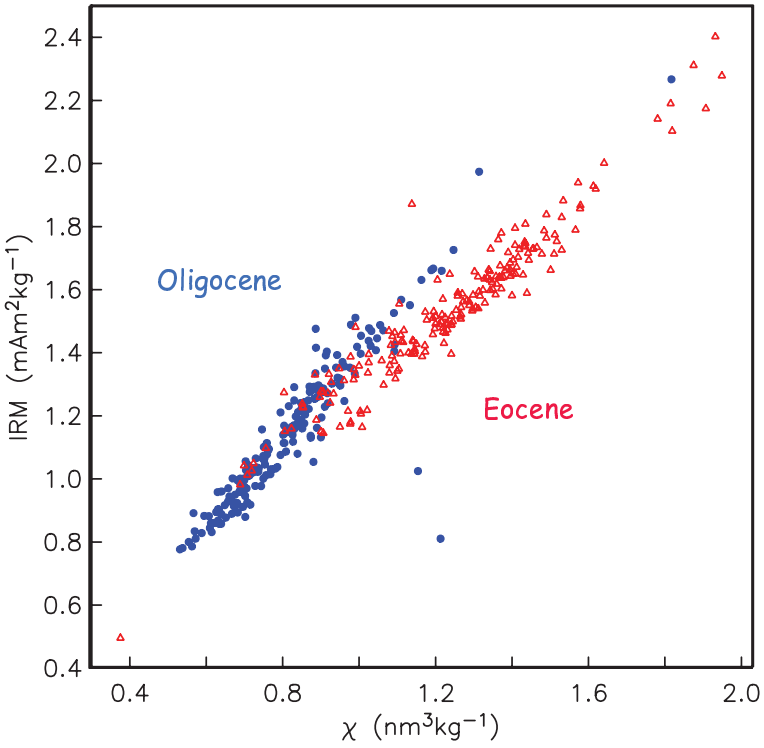


Figure 8.18: Saturation IRM versus magnetic susceptibility $\chi$ for Hole 522 across the Eocene/Oligocene boundary. The Eocene group (red triangles) plots along a line of lower IRM/$\chi$ compared to the Oligocene group (blue circles).

# Appendix

## A Fourier analysis of hysteresis loops

In practice, hysteresis measurements may yield rather noisy data. Jackson et al. [1990] suggested that noisy hysteresis data could be filtered using a Fourier transform. The advantages of Fourier smoothing are that the calculated hysteresis parameters are less sensitive to noise and that the $\Delta M$ and $d\Delta M/dH$ curves are more readily interpreted.

The steps involved in Fourier smoothing of hysteresis loops are as follows (see Figure A1):

- First, the contribution of paramagnetic and diamagnetic phases must be removed. Figure A1a shows some typical data from carbonate rich sediments. These samples have a strong diamagnetic (negative high field slope) contribution. We remove the diamagnetic contribution by calculating a best-fit line using linear regression for the data at high fields (after the ferromagnetic phases have reached saturation) and removing its contribution by subtraction (see Figure A1b).

- In order to ensure uniformity of data treatment, Jackson et al. [1990] recommend truncating the data at some fixed percentage of $M_s$ (after slope adjustment). We truncate the data at 99.9% of $M_s$ in Figure A1b.

- A Fourier transform requires data with a single $y$ value for every $x$ value and hysteresis data, as normally plotted are not suitable. The loops can be mapped into a suitable form for Fourier analysis by transforming the field values into radians, as shown in Figure A1c. The unfolded loop starts at the point when the descending curve intersects the $y$ axis ($M_r$). From $H = 0 \rightarrow -H_{\max}$, $H$ is mapped linearly to radians ($H' = 0 \rightarrow \pi/2$). From $H = -H_{\max} \rightarrow 0$, $H$ is mapped to $H' = \pi/2 \rightarrow \pi$. From $H = 0 \rightarrow +H_{\max}$, we map $H$ to $H' = \pi \rightarrow 3\pi/2$, and finally, for $H = +H_{\max} \rightarrow 0$, $H$ is converted to $H' = 3\pi/2 \rightarrow 2\pi$.

- The "unfolded" data can then be subjected to a Fourier Transform as described by Jackson et al. [1990]. The data can be smoothed by retaining only a specified number of terms (see Figure A1d). Finally, hysteresis parameters can be calculated from the reconstituted loop and $\Delta M$ and $d\Delta M/dH$ curves can be plotted (see Figure A1e-f).

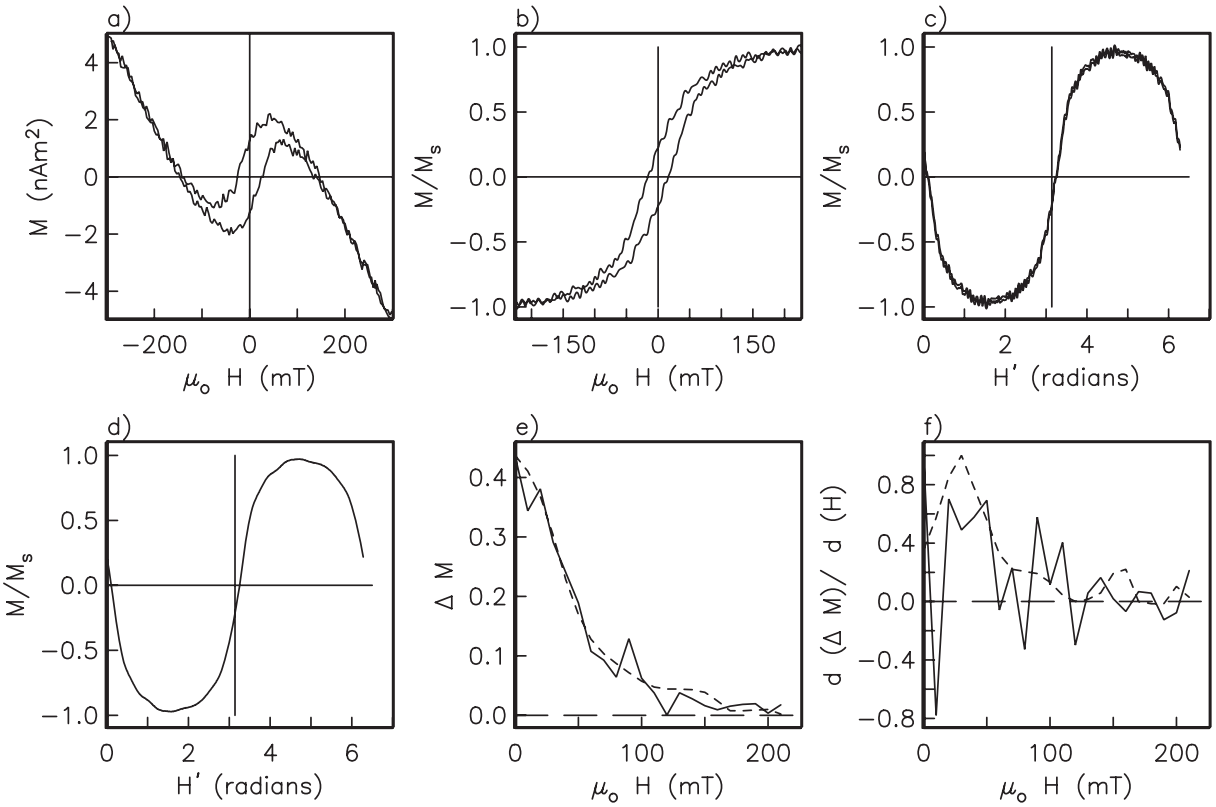


Figure A1: Steps in Fourier smoothing: a) the original data - note the negative high field slope from the diamagnetic contribution of carbonate, b) data with the high field slope removed and truncated to 99.9% of the maximum value of $M$, c) data from b) "unfolded" into radians, d) data from c) smoothed by using the first 15 terms of Fourier series, e) comparison of $\Delta M$ curve using original data (solid line) and smoothed data (dashed line), f) comparison of the $d\Delta M/dH$ curve using the original data (solid line) and smoothed data (dashed line).

# Bibliography


Banerjee, S. K., King, J. & Marvin, J. (1981), 'A rapid method for magnetic granulometry with applications to environmental studies', *Geophys. Res. Lett.* **8**, 333–336.

Day, R., Fuller, M. D. & Schmidt, V. A. (1977), 'Hysteresis properties of titanomagnetites: grain size and composition dependence', *Phys. Earth Planet. Inter.* **13**, 260–266.

Dunlop, D. (2002), 'Theory and application of the day plot ($m_{rs}/m_s$ versus $h_{cr}/h_c$) 2. application to data for rocks, sediments, and soils', *J. Geophys. Res* **107**, doi:10.1029/2001JB000487.

Dunlop, D. & Argyle, K. (1997), 'Thermoremanence, anhysteretic remanence and susceptibility of submicron magnetites: Nonlinear field dependence and variation with grain size', *J. Geophys. Res* **102**, 20199–20210.

Egli, R. (2003), 'Analysis of the field dependence of remanent magnetization curves', *Journal of Geophysical Research-Solid Earth* **108**(B2).

Evans, M. & Heller, F. (2003), *Environmental Magnetism: Principles and Applications of Enviromagnetics*, Academic Press.

Fabian, K. (2003), 'Some additional parameters to estimate domain state from isothermal magnetization measurements', *Earth and Planetary Science Letters* **213**(3-4), 337–345.

Hartl, P., Tauxe, L. & Herbert, T. (1995), 'Eartliest oligocene increase in south atlantic productivity as interpreted from "rock magnetics" at dsdp site 522', *Paleoceanography* **10**, 311–325.

Heider, F., Zitzelsberger, A. & Fabian, K. (1996), 'Magnetic susceptibility and remanent coercive force in grown magnetite crystals from 0.1 $\mu$m to 6mm', *Phys. Earth Planet. Inter.* **93**, 239–256.

Hunt, C. P., Moskowitz, B. M. & Banerjee, S. K. (1995), 'Rock physics and phase relations, a handbook of physical constants', pp. 189–204.

Jackson, M., Worm, H. U. & Banerjee, S. K. (1990), 'Fourier analysis of digital hysteresis data: rock magnetic applications', *Phys. Earth Planet. Inter.* **65**, 78–87.

Kruiver, P. P., Dekkers, M. J. & Heslop, D. (2001), 'Quantification of magnetic coercivity components by the analysis of acquisition curves of isothermal remanent magnetisation', *Earth and Planetary Science Letters* **189**(3-4), 269–276.

Lowrie, W. (1990), 'Identification of ferromagnetic minerals in a rock by coercivity and unblocking temperature properties', *Geophys. Res. Lett.* **17**, 159–162.

Maher, B. A. & Thompson, R., eds (1999), *Quaternary Climates, Environments and Magnetism*, Cambridge University Press.

Mayergoyz, I. (1986), 'Mathematical models of hysteresis', *IEEE Trans. Magn.* **MAG-22**, 603–608.

Pike, C. R., Roberts, A. P., Dekkers, M. J. & Verosub, K. L. (2001), 'An investigation of multi-domain hysteresis mechanisms using forc diagrams', *Physics of The Earth and Planetary Interiors* **126**(1-2), 11–25.

Pike, C., Roberts, A. & Verosub, K. (1999), 'Characterizing interactions in fine magnetic particle systems using first order reversal curves', *J. Appl. Phys.* **85**, 6660–6667.

Robertson, D. J. & France, D. E. (1994), 'Discrimination of remanence-carrying minerals in mixtures, using isothermal remanent magnetisation acquisition curves', *Physics of The Earth and Planetary Interiors* **82**(3-4), 223–234.

Tauxe, L., Bertram, H. & Seberino, C. (2002), 'Physical interpretation of hysteresis loops: Micromagnetic modelling of fine particle magnetite', *Geochem., Geophys., Geosyst.* **3**, DOI 10.1029/2001GC000280.

Tauxe, L., Mullender, T. A. T. & Pick, T. (1996), 'Potbellies, wasp-waists, and superparamagnetism in magnetic hysteresis', *Jour. Geophys. Res.* **101**, 571–583.

Yu, Y. & Tauxe, L. (2004), 'On the use of magnetic transient hysteresis in paleomagnetism for granulometry', *Geochem., Geophys., Geosyst.* **6**, Q01H14; doi: 10.1029/2004GC000839.